European Journal of Pharmaceutics and Biopharmaceutics 142 (2019) 460–472

Contents lists available at ScienceDirect

European Journal of Pharmaceutics and Biopharmaceutics

journal homepage: www.elsevier.com/locate/ejpb

Research paper

Verapamil delivery systems on the basis of mesoporous ZSM-5/KIT-6 and ZSM-5/SBA-15 polymer nanocomposites as a potential tool to overcome MDR in cancer cells

Margarita Popova[a,*], Rositsa Mihaylova[b], Georgi Momekov[b], Denitsa Momekova[b], Hristina Lazarova[a], Ivalina Trendafilova[a], Violeta Mitova[c], Neli Koseva[c], Judith Mihályi[d], Pavletta Shestakova[a], Petko St. Petkov[e], Hristiyan A. Aleksandrov[e], Georgi N. Vayssilov[e], Spiro Konstantinov[b], Ágnes Szegedi[d,*]

[a] Institute of Organic Chemistry with Centre of Phytochemistry, Bulgarian Academy of Sciences, 1113 Sofia, Bulgaria
[b] Faculty of Pharmacy, Medical University Sofia, Bulgaria
[c] Institute of Polymers, Bulgarian Academy of Sciences, 1113 Sofia, Bulgaria
[d] Research Centre for Natural Sciences, Institute of Materials and Environmental Chemistry, Hungarian Academy of Sciences, 1117 Budapest, Magyar tudósok körútja 2, Hungary
[e] Faculty of Chemistry and Pharmacy, University of Sofia, 1126 Sofia, Bulgaria

ARTICLE INFO

Keywords:
Zeolite/mesoporous silica nanocomposites
Surface modification
Verapamil
Delivery systems
Multi-drug resistance

ABSTRACT

ZSM-5/KIT-6 and ZSM-5/SBA-15 nanoparticles were synthesized and further modified by a post-synthesis method with $-(CH_2)_3SO_3H$ and $-(CH_2)_3NHCO(CH_2)_2COOH$ groups to optimize their drug loading and release kinetic profiles. The verapamil cargo drug was loaded by incipient wetness impregnation both on the parent and modified nanoporous supports. Nanocarriers were then coated with a three-layer polymeric shell composed of chitosan-k-carrageenan-chitosan with grafted polysulfobetaine chains. The parent and drug loaded formulations were characterized by powder XRD, N_2 physisorption, thermal analysis, AFM, DLS, TEM, ATR-FT-IR and solid state NMR spectroscopies. Loading of verapamil on such nanoporous carriers and their subsequent polymer coating resulted in a prolonged *in vitro* release of the drug molecules. Quantum-chemical calculations were performed to investigate the strength of the interaction between the specific functional groups of the drug molecule and $-(CH_2)_3SO_3H$ and $-CH_2)_3NHCO(CH_2)_2COOH$ groups of the drug carrier. Furthermore, the ability of the developed nanocomposites to positively modulate the intracellular internalization and thereby augment the antitumor activity of the p-gp substrate drug doxorubicin was investigated in a comparative manner *vs.* free drug in a panel of MDR positive (HL-60/Dox, HT-29) and MDR negative (HL-60) human cancer cell lines using the Chou-Talalay method.

1. Introduction

Drug encapsulation inside nanoporous materials (zeolites, mesoporous silicas, etc.) and their possible application as new generation therapeutics, theranostic platforms or smart devices is of increasing interest due to their expanding capacity to successfully address delivery related problems [1–10]. Recently, mesoporous silicas and zeolites have attracted much notice owing to their unique features including synthetically controllable architecture of the pores and pore size diameter, large surface area and possible functionalization of the materials surface. Nanoporous particles have now been used in a broad range of pharmaceutical applications, either as drug delivery platform for novel diagnostic systems. In addition, appropriate design of nanoscale host units based on these materials can help to solve some major problems associated with low stability and poor bioavailability of various bioactive molecules [11–13]. Further development of a new generation advanced nanoscale therapeutics requires complete understanding and control over the complex host–guest interactions of the organic molecules confined within nanosized chambers at different length scales. Numerous studies show that proper surface modification of the silica matrix with organic functional groups could further improve the loading efficacy and optimize the release kinetics of the cargo drug. To

* Corresponding authors.
E-mail addresses: mpopova@orgchm.bas.bg (M. Popova), szegedi.agnes@ttk.mta.hu (Á. Szegedi).

https://doi.org/10.1016/j.ejpb.2019.07.021
Received 17 February 2019; Received in revised form 10 July 2019; Accepted 19 July 2019
Available online 20 July 2019
0939-6411/

closely control these processes, mesoporous silica carriers could be advantageously modified depending on the structural functionality of the hosted drug with different organic groups (chloropropyl, phenyl, benzyl, mercaptopropyl, cyanopropyl, butyl radicals) [3,4,10]. Moreover the appropriate surface functionalization of mesoporous silicas is prerequisite for their further successful inclusion in composites obtained by their integration with polymers. Despite of the outstanding features of the microporous structure of zeolites and the presence of stronger adsorption sites [9], the sole presence of micropores often imposes significant limitations. Drug loading in the small pores of microporous carriers is seriously limited and only 10% of zeolite adsorption sites can be accessible for adsorption [7,9]. The use of hierarchical zeolites can solve some of these problems. Composite zeolite/mesoporous silica materials combine the interconnected networks of zeolite micropores with structured mesopores, as well as the stability and acidic properties of zeolites, offering good possibilities for interaction with drugs with suitable functionality [10]. An additional polymer coating of the zeolite/mesoporous silica composite could be applied in order to increase their physical stability and, on the other hand, to achieve sustained drug release and to decrease the initial burst-effect observed for non-coated counterparts [3,10].

Verapamil (Scheme 1), an L-type calcium channel blocker of the phenylalkylamine class, has been widely used in the clinical management of hypertension, angina pectoris, cardiac arrhythmias, and most recently, migraine and cluster headaches. [14–16]. Its chemosensitizing properties were first recognized in multi-drug resistant leukemia cells by which a 10-fold increase in the cellular concentration of the p-gp substrate drug vincristine was observed. Later on, reversal of acquired or intrinsic resistance to vinca alkaloids and anthracycline antibiotics by verapamil has successfully been demonstrated in MDR-1 overexpressing animal and human cell lines [8,17]. Unfortunately at the doses associated with MDR-modulation verapamil poses significant risk of side effects, as it requires several fold higher concentrations as a chemosensitizing agent, *vs.* its therapeutic levels as an antiarrhytmic drug [8]. This makes it a suitable candidate for incorporation in targeted formulations to justify its loading in silica mesoporous nanocarriers to ensure passive targeting to tumors using the enhanced premeation and retention (EPR) effect [18]. As evidenced, a primary determinant of the MDR-resistant phenotype of numerous tumor types is the reduced intracellular drug accumulation due to abnormal expression of specific membrane transporters of the ATP-binding cassette (ABC) superfamily that renders tumor cells resistant to a broad spectrum of chemically unrelated drugs (anthracylclines, vinca-alkaloids, podophyllotoxin derivatives, taxanes etc.) [19]. Of greatest clinical importance appear to be the multidrug transporter (MDR-1) or P-glycoprotein (P-gp) proved to be up-regulated in colorectal carcinoma cells (HT-29), as well as the ATP-dependent glutathione S-conjugate carrier MRP-1 that has been recognized as a hallmark mechanism of MDR in acute myeloid leukemic cells (HL-60). Therefore, pharmacological modulation of the efflux transport activity has widely been explored as a therapeutic strategy to circumvent tumor drug resistance. A further step in reversing the MDR phenotype in malignant cells includes the design and synthesis of analogous ABC transporter inhibitors with greater specificity and lower toxicity as well as exploring the use of various delivery platforms (i.e. liposomes, polymer nanoparticles, mesoporous silica, etc.) for the first generation prototypes such as verapamil.

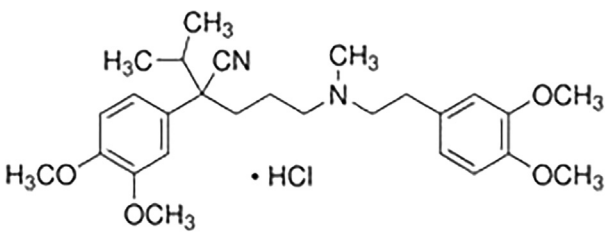

Scheme 1. Verapamil hydrochloride.

To investigate the intracellular trafficking of the p-gp substrate drug doxorubicin, we herein report on the synthesis, *in vitro* release kinetics and synergistic effects of verapamil-loaded parent and $-(CH_2)_3SO_3H$ or $-(CH_2)_3NHCO(CH_2)_2COOH$-modified ZSM-5/KIT-6 and ZSM-5/SBA-15 nanocomposites. The latter were coated with a three-layer polymer shell composed of chitosan-κ-carrageenan-chitosan with grafted polysulfobetaine chains. The chemosensitizing properties of the obtained nanoparticles to doxorubicin was investigated in a comparative way *vs.* free verapamil drug in a panel of MDR positive (HL-60/Dox, HT-29) and MDR negative (HL-60) human cancer cell lines. Potential synergistic benefits of the tested drug combinations were evaluated using the Chou-Talalay method (CTM) that is now widely acknowledged as a milestone in studying drug interactions.

2. Materials and methods

The chemicals used for synthesis were tetraethyl orthosilicate (TEOS, 99%, Aldrich), tetrapropylammonium hydroxide (TPAOH, 20% in water, Aldrich), aluminum isopropoxide (AlIP, 98%, Aldrich), triblock copolymer pluronic P123 (EO20PO70EO20, MW = 5800 g/mole, Aldrich), hydrochloric acid (HCl, 37% in water, J.T. Baker), ammonium hydroxide (25% of NH_3 in water, Acros), Cumene (98%, Aldrich), and 1,3,5-tri-isopropyl benzene (TIPB, 96%, Aldrich). The reagents used for the synthesis of the polysulfobetaine: [2- (methacryloyloxy) ethyl]dimethyl-(3-sulfonyl)ammonium hydroxide, 4-(hydroxymethyl)-1,3-dioxolan-2-one, 2-bromo-2-methylpropionyl bromide, CuBr, 2,2′-dipyridyl, triethylamine, dimethyl aminopiridine chloroform and trifluoroethanol were provided by Sigma-Aldrich. Chitosan and k-carrageenan were also supplied from Sigma-Aldrich. Triethylamine and chloroform (stirred over CaH) were distilled prior use. All other reagents were used as received without further purification.

2.1. Synthesis of ZSM-5/KIT-6 and ZSM-5/SBA-15 nanocomposite

The synthesis procedure [20] with some modifications was performed in two stages. Seed solutions are synthesized and pre-crystallized as a first step. After that the fraction of precursors in the presence of a supramolecular template was transformed into an ordered mesoporous aluminosilicate. A typical synthesis gel content is: 6.0 g of TEOS, 5.0 g of TPAOH, 7.0 g of distilled H_2O, and 0.19 g of AlIP.

(a) Synthesis of ZSM-5/KIT-6

The ingredients were mixed at room temperature for 5 h and stirred overnight to complete the hydrolysis process, followed by pre-crystallization at 363 K for 24 h in a reflux system. The P123 solution was simultaneously prepared by dissolving 2.0 g of P123 in 75 ml of 1.6 M HCl at room temperature and stirring for 4 h until a clear solution was obtained. Then, the ZSM-5 precursor solution prepared as described above was added dropwise to the P123 solution, followed by aging at 313 K for 24 h. pH value was adjusted to 3.5 with aqueous NH_3 solution before transferring the mixture into a teflon-lined autoclave for more incorporated aluminum and further silica condensation at 473 K for 24 h. The final product was filtered off, washed with distilled water, and dried at 373 K for 12 h. The as-synthesized material was calcined in air at 823 K for 5 h with a heating rate of 2 K/min to remove the organic template. The obtained material was denoted as ZSM-5/KIT-6.

(b) Synthesis of ZSM-5/SBA-15

The ingredients were mixed at room temperature and stirred at 363 K for 24 h in a reflux system. The P123 solution was simultaneously prepared by dissolving 2.0 g of P123 in 61 ml of distilled H_2O and 6.2 g 37% HCl at room temperature and stirring for 4 h until a clear solution

was obtained. Then, the ZSM-5 precursor solution prepared as described above was added dropwise to the P123 solution, followed by aging at 313 K for 24 h. After that the solution was transferred into a teflon-lined autoclave at 473 K for 24 h. The final product was filtered off, washed with distilled water, and dried at 373 K for 12 h. The as-synthesized material was calcined in air at 823 K for 6 h with a heating rate of 1 K/min to remove the organic template. The obtained material was denoted as ZSM-5/SBA-15.

2.2. Functionalization of ZSM-5/KIT-6 and ZSM-5/SBA-15 nanocomposites with $-(CH_2)_3SO_3H$ and $-(CH_2)_3NHCO(CH_2)_2COOH$ groups

The initial ZSM-5/KIT-6 and ZSM-5/SBA-15 nanocomposites were functionalized with 3-mercaptopropyl trimethoxysilane by dispersing in toluene at refluxed condition for 6 h and then filtered, washed, and dried in oven at 328 K for 3 h. Further, the obtained mercapto-modified mesoporous silicas were dispersed in H_2O_2 and stirred for 24 h at room temperature. The oxidized materials were filtered and dried in a vacuum oven at 323 K for 8 h and denoted as ZSM-5/KIT-6-SO_3H and ZSM-5/SBA-15-SO_3H nanocomposites, respectively.

Modification of the initial ZSM-5/KIT-6 and ZSM-5/SBA-15 nanocomposites with amino groups was accomplished by reaction with 3-amino-propyltriethoxysilane (APTES) in ethanol (5 h, 323 K) and in anhydrous toluene (24 h, 333 K), respectively. Samples were washed with several portions of solvent, and finally with water and dried at room temperature. The reaction of amino modified silicas with succinic anhydride was carried out in toluene. To remove adsorbed water azeotropic drying of amino modified silicas was made at 388 K by mixing 1 g of silica with 20 ml of anhydrous toluene. 6.6 mmol of succinic anhydride (assuming 2 wt% of amino content on silica) was added to the mixture at 333 K and treated for 24 h. The samples were dried by vacuum evaporation (0.04 Pa) at room temperature for 6 h and denoted as ZSM-5/KIT-6-COOH and ZSM-5/SBA-15-COOH nanocomposites, respectively.

2.3. Verapamil loading

The ZSM-5/KIT-6-SO_3H(COOH) and ZSM-5/SBA-15-SO_3H(COOH) nanocomposites were loaded with verapamil by incipient wetness impregnation. ZSM-5/KIT-6 and ZSM-5/SBA-15 nanocomposites and verapamil in weight ratio 1.0:0.5 were stirred in 1 ml ethanol until total evaporation of the solvent. Then 0.5 g of powder product was washed three times with 50 ml of distilled water, and dried at 313 K overnight. The preparations obtained were designated as Ver/ZSM-5/KIT-6-SO_3H(COOH) and Ver/ZSM-5/SBA-15-SO_3H(COOH).

2.4. Coating by polymer complex

(a) Synthesis of polysulfobetaine with terminal cyclic carbonate groups.

The monomer [2- (methacryloyloxy) ethyl]dimethyl-(3-sulfonyl) ammonium hydroxide and the initiator 2-oxo-1,3-dioxolan-4-yl-(methyl-2-bromo-2-methylpropionate) (In) in molar ratio 35:1 and trifluoroethanol (2 ml) were placed in a reactor. The solution was degassed 3 times by a freeze–thaw process. To the mixture CuBr and 2,2′-dipyridyl were added. The molar ratio of the initiator and the catalyst was In:CuBr:2,2′-dipyridine = 1:1:2. Three freeze–thaw cycles were applied. The reaction was carried out for 14 h at 333 K. The reaction mixture was diluted with distilled water (1:1) and the product precipitated in methanol (50 ml). The polymer obtained was dissolved in distilled water (5 ml) and dialyzed (MWCO 3 500) for 72 h against distilled water. Mn = 10500 g/mol, Mw/Mn = 1.48 (determined by gel permeation chromatography). It was denoted as PSB.

(b) Synthesis of chitosan with grafted polysulfobetaine chains

To 10 ml chitosan solution (20 mg/ml, pH ~ 6) was added 1 ml PSB solution (200 mg/ml) and stirred for 5 days at room temperature. The solution was then dialyzed (MWCO 12-14000) for a further 5 days and lyophilized. Yield 250 mg (grafting rate 25%). The product was designated as chitosan-PSB.

(c) Coating of silica nanoparticles with polylectrolyte complexes

Aqueous solutions of chitosan, chitosan-PSB and k-carrageenan at a concentration of 0.5% and pH = 5 were prepared. To 50 mg of loaded particles, Ver/ZSM-5/KIT-6SO_3H(COOH) or Ver/ZSM-5/SBA-15SO_3H(COOH), 2.5 ml of the polysaccharide solutions were added in the following sequence: the chitosan solution, after drying at room temperature and under reduced pressure the k-carrageenan solution was added followed by drying and then the third chitosan-PSB solution was added. The particles were dried under reduced pressure to a constant weight. The samples were denoted as Ver/ZSM-5/KIT-6-COOH/P; Ver/ZSM-5/SBA-15-COOH/P; Ver/ZSM-5/KIT-6-SO_3H/P and Ver/ZSM-5/SBA-15-SO_3H/P.

2.5. Characterization

X-ray powder diffraction patterns were recorded on a Philips PW 1810/3710 diffractometer with Bragg-Brentano parafocusing geometry applying monochromatized Cu K_α (λ = 0.15418 nm) radiation (40 kV, 35 mA) and proportional counter.

Nitrogen physisorption measurements were carried out at 77 K using Tristar 3000 Micromeritics volumetric adsorption analyzer. Before the adsorption analysis, the silica sample was outgassed under vacuum for 2 h at 473 K, while modified and drug loaded samples were pretreated at 353 K for 5 h.

Thermogravimetric measurements were performed with a Setaram TG92 instrument with a heating rate of 5 K/min in air flow.

Attenuated Total Reflection Infrared (ATR-FT-IR) spectra were recorded on a Varian Scimitar 2000 FT-IR spectrometer equipped with a MCT (mercury-cadmium-tellur) detector and a single reflection ATR unit (SPECAC “Golden Gate”) with diamond ATR element. In general, 128 scans and 4 cm^{-1} resolution was applied. For all spectra ATR-correction was performed (Varian ResPro 4.0 software).

The atomic force microscopy (AFM) measurements were performed on a Bruker Dimension Icon instrument equipped with a NanoScope V Control Station (Bruker Nanosurface Division, USA) operating in a tapping mode in air. The SPM Scan Head has a XY nominal range of 90 × 90 μm and a Z range of 10 μm. The samples were imaged at room temperature and at least 24 h after spin-coating.

TEM images were taken using a MORGAGNI 268D TEM (100 kV; W filament; 153 point-resolution = 0.5 nm).

Solid-state NMR spectra were measured on a Bruker Avance II + 600 NMR spectrometer equipped with a 4 mm dual $^1H/X$ broadband CPMAS probe with operating frequency for ^1H 600.01 MHz (156.34 MHz for ^{27}Al, 150.87 MHz for ^{13}C and 119.21 MHz for ^{29}Si). The following experimental parameters were used for ^{27}Al magic-angle spinning (MAS) measurements - excitation pulse of 2.5 μs, number of scans 12,000 and relaxation delay between scans 0.5 s, MAS rate 12 kHz. For $^1H \rightarrow {}^{13}C$ cross-polarization MAS (CPMAS) experiment the MAS rate was 6 kHz, ^1H excitation pulse of 3.6 μs was used, 2 ms contact time, 5 s relaxation delay, 9000 scans. For $^1H \rightarrow {}^{29}Si$ cross-polarization MAS (CPMAS) experiment, ^1H excitation pulse of 3.6 μs was used, 5 ms contact time, 5 s relaxation delay, 10,000 scans, MAS rate 10 kHz. ^1H SPINAL-64 decoupling scheme was used during acquisition of the CP experiments.

Dynamic light scattering (DLS) measurements were carried out at 298 K on a Brookhaven BI-200 goniometer with vertically polarized incident light at a wavelength λ = 632.8 nm supplied by a He-Ne laser

operating at 35 mW and equipped with a Brookhaven BI-9000 AT digital autocorrelator. The hydrodynamic size (D_h) of the particles was determined in an aqueous solution with concentration 1 mg/mL at scattering angle θ = 90°. Prior measurements the solution was sonicated for 10 min.

2.6. In-vitro release study

An *in vitro* verapamil release study was performed in a phosphate buffered solution pH = 7 at 310 K. The verapamil-loaded particles (2 mg) were incubated in 50 ml buffer at 310 K under stirring (100 rpm). At appropriate time intervals, 3 ml samples were withdrawn from the release medium and analyzed with UV–Vis spectroscopy at a wavelength of 272 nm. The concentration of the released verapamil was calculated according to the standard curve prepared in phosphate buffer ($r > 0.9993$).

2.7. Cell lines and culture conditions

In vitro cytotoxicity was assessed in a panel of tumor cell lines with varying chemosensitivity towards doxorubicin that correlates with overexpression of specific membrane transporters of the ATP-binding cassette (ABC) superfamily: MDR-1 overexpressing colorectal adenocarcinoma cells (HT-29); MDR negative AML cell line (HL-60) and its correspondent multidrug-resistant strain (HL-60/Dox) with an induced MRP-1 expression.

All tumor cell lines were purchased from the German Collection of Microorganisms and Cell Cultures (DSMZ GmbH, Braunschweig, Germany). The MDR phenotype of the HL-60/Dox subline was induced at the Laboratory of Experimental Chemotherapy (Faculty of Pharmacy, MU-Sofia). Selection has been carried out by prolonged serial exposures of the maternal cell line HL-60 to gradually increasing concentrations of doxorubicin. The established multidrug-resistant phenotype has been sustained through cell cultivation in a growth medium containing 0.2 μM doxorubicin. Resistant cells were incubated in a drug-free environment at least five days prior to the experiment to avoid possible synergistic interactions with the being screened for cytotoxicity compounds.

All cell cultures were cultivated in a growth medium RPMI 1640 supplemented with 10% fetal bovine serum (FBS), 5% L-glutamine and incubated under standard conditions of 310 K and 5% humidified CO_2 atmosphere.

2.8. Cytotoxicity assessment (MTT-dye reduction assay).

Experiment design involved a number of cytotoxicity assays that measured cell growth inhibition by doxorubicin and verapamil alone as well as the boosting effect of free verapamil or verapamil-loaded ZSM-5/KIT-6-SO_3H(COOH) and ZSM-5/SBA-15-SO_3H(COOH) nanocomposites on the cellular kinetics of doxorubicin when treated concomitantly. Cell viability was evaluated using a standard MTT-based colorimetric assay. Exponential-phased cells were harvested and seeded (100 μl/well) in 96-well plates at the appropriate density, i.e. 3×10^5 for the suspension culture HL-60, HL-60/Dox and 1.5×10^5 for the adherent one HT-29. All three tumor cell lines were treated as specified in the following section. After exposure time of 72 h, filter sterilized MTT substrate solution (5 mg/ml in PBS) was added to each well of the culture plate. A further 1–4-h incubation allowed formation of purple insoluble precipitates of the formazan dye. The latter were dissolved in isopropyl alcohol solution containing 5% formic acid prior to absorbance measurement at 550 nm. Collected absorbance values were blanked against MTT-and isopropanol solution and normalized to the mean value of untreated control (100% cell viability).

2.9. Chou-Talalay method

The establishment and quantitative evaluation of the synergistic interactions in the conducted assays was based on the Chou-Talalay method and its respective CompuSyn® software. The "dose-response" relationships were derived in advance *via* the standard MTT test, following 72 h exposure to doxorubicin in the presence of free verapamil substance or verapamil-loaded mesoporous silica nanoparticles S1/2/3/4 in fixed 1:1 or varying ratio combinations, respectively. Treatment concentrations were selected with regard to the different chemosensitivity of the screened tumor cell lines, as follows:

In the referent 1:1 fixed ratio combination study, all tumor cell types (HL-60, HL-60/Dox, HT-29) were treated with 5-fold serial dilutions of doxorubicin and free verapamil in the concentration range of 40.0–2.5 μM. The boosting effect of verapamil on the intracellular accumulation of doxorubicin was evaluated against the single drug effects of the antibiotic in the same concentration range.

A different non-fixed ratio protocol was used for the synergism study of the experimental verapamil formulations S1/2/3/4. Thereby, the fixed concentration dose of doxorubicin was determined based on the toxicity profile of the single drug in the screened tumor models. The parental HL-60 cells received half maximal inhibitory concentration of doxorubicin (15 μM), whereas the *ab initio* resistant variant HL-60/Dox and the colorectal cancer cell line HT-29 were treated with twice as high concentrations (30 μM) that closely resemble the estimated IC_{50} values of doxorubicin. Synergism was evaluated at varying treating doses of the studied polymers S1, S2, S3 and S4 equivalent to the non-cell-toxic 10.00 μM, 5.00 μM, 2.00 μM, 1.00 μM and 0.5 μM concentrations of the loaded verapamil.

In all combination scenarios, the nature of the studied drug interactions was determined based on the automatically calculated CI and DRI indices at actual experimental data points (fixed- and varying ratio experiments) and for each dataset of the simulated dose-response curve (fixed ratio experiments).

The accessory CompuSyn®software performs an automated analysis of actual and simulated dose-response data and generates a plot of combination index (CI) values against different fractions affected (Fa). The CI provides a quantitative determination of a synergistic ($CI < 1$), additive ($CI = 1$), and antagonistic ($CI > 1$) drug behaviour in fixed- or varying-ratio combinations. Similarly, a DRI (dose reduction index)-Fa plot indicates the extent (folds) to which a single-drug dose may be reduced when used in a combination, without compromising the initial response it produced. Corresponding isobolograms are also constructed and can be used as an accessory tool in evaluating drug performance [21].

2.10. Method and models

We performed quantum-chemical calculations using the program Gaussian 09 [22]. The hybrid density functional M06-2X [23] with 6-$31+G^{**}$ type of basis sets is used for all atoms. All modeled systems were considered solvated in water solution, as the solvent effects were taken into account by the long-range electrostatic effect using the polarizable continuum model (PCM) [24].

The binding energies (BE) of the adsorbed verapamil molecule to the substrate represented by acid molecules are calculated as $BE = -E_{ad} - E_{sub} + E_{ad/sub}$, where E_{ad} is the total energy of the verapamil adsorbate in the gas phase, E_{sub} is the total energy of the substrate (acid molecules), and $E_{ad/sub}$ is the total energy of the substrate (acid molecules) interacting with the adsorbed verapamil molecule. Hence, negative values of BE imply favorable (exothermic) interaction between the verapamil molecule and the substrate (acid molecules).

The calculated frequencies are scaled by 0.952 [https://cccbdb.nist.gov/vibscalejust.asp]

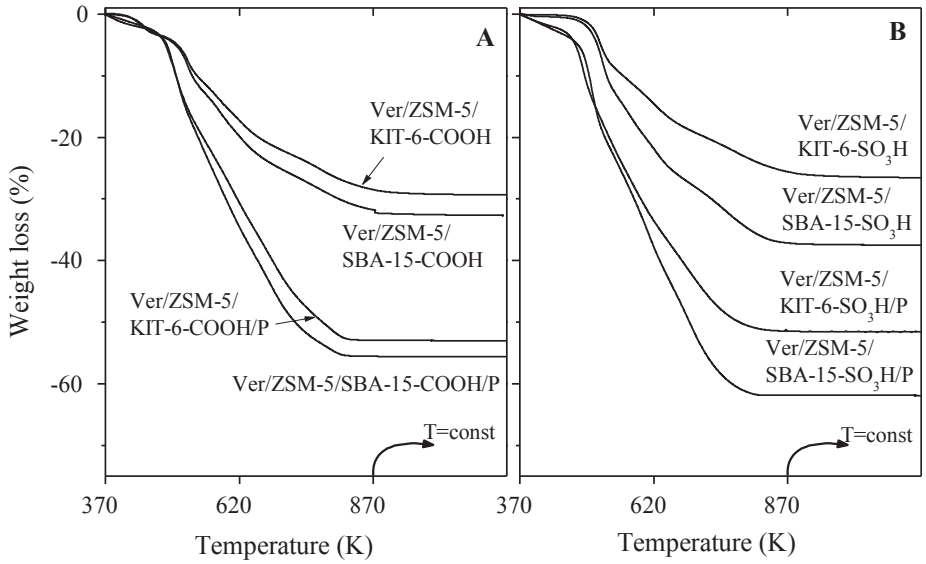

Fig. 1. TG analysis of verapamil ZSM-5/KIT-6-COOH (A) and ZSM-5/KIT-6-SO_3H (B) formulations.

3. Results and discussion

3.1. Verapamil loading into the ZSM-5/KIT-6 and ZSM-5/SBA-15 nanocomposites

Verapamil was loaded on zeolite/mesoporous silica carriers by incipient wetness impregnation. The amount of the functional $-CH_3(CH_2)_2SO_3H$ and $-(CH_2)_3NHCO(CH_2)_2COOH$ groups, of the loaded verapamil and of the polymer coating was determined by thermogravimetric method (Fig. 1). The calculated amount of $-CH_3(CH_2)_2SO_3H$ groups bound to the surface of ZSM-5/KIT-6 and ZSM-5/SBA-15 is 7.3 wt% and 4.0 wt%, respectively, whereas the amount of $-(CH_2)_3NHCO(CH_2)_2COOH$ groups connected to the surface of the corresponding nanoparticles is 12.5 wt% and 11.3 wt%, respectively (Table 1). The TG analysis determined the actual amount of verapamil in the carriers after correcting the curves for water and functional groups content. TG data show that the amount of verapamil loaded on ZSM-5/KIT-6-SO_3H and ZSM-5/SBA-15-SO_3H samples is 21.3 and 33.6 wt%, respectively, and on ZSM-5/KIT-6-COOH and ZSM-5/SBA-15-COOH samples is 17.1 and 19.4 wt%, respectively (Table 1).

The lower amount of loaded drug in ZSM-5/KIT-6 material could be explained with its more ordered 3D pore systems with interconnected channels, where the penetration of the drug molecules is hindered within the narrow pore entrances. The long chains with the carboxylic groups at the end ($-(CH_2)_3NHCO(CH_2)_2COOH$) on ZSM-5/KIT-6 additionally restrict the access to the pores. The highest drug adsorption (33.6 wt%) was achieved for ZSM-5/SBA-15 modified with $-(CH_2)_3SO_3H$ groups due to the more open structure of the nanocarrier and shorter modification segments.

3.2. Structural characteristics of the $-(CH_2)_3SO_3H$ and $-(CH_2)_3NHCO(CH_2)_2COOH$ modified composites and loaded materials

The aluminum content determined by elemental analysis is 0.8 wt% for ZSM-5/KIT-6 and 0.3 wt% for ZSM-5/SBA-15. TEM images show the presence

Parent ZSM-5/KIT-6 and ZSM-5/SBA-15 materials were characterized by solid state ^{27}Al NMR spectroscopy (Supplementary data Fig. SD1 a and b). The ^{27}Al spectrum of ZSM-5/KIT-6 material (Supplementary data, Fig. SD1a) shows two resonances at 57 ppm and at around 0 ppm. The intense signal centered at 57 ppm is characteristic for framework Al species in tetrahedral coordination (AlO_4 structural unit), whereas the low intensity broad resonance at 0 ppm indicates the presence of small amount of six-coordinated aluminum species and defect framework Al sites (AlO_6 structural units). The calculated Al^{IV}/Al^{VI} ratio was 3.8, indicating the presence of predominantly tetra-coordinated Al framework units, which is a proof for the preservation of ZSM-5 structure in the ZSM-5/KIT-6 composites.

The ^{27}Al spectrum of ZSM-5/SBA-15 sample (Supplementary data, Fig. SD1b) displays a very broad resonance covering the range from 170 to −60 ppm centered at around 30 ppm and overlapped with a sharper signal at around 58 ppm. This observation indicates that during the preparation of ZSM-5/SBA-15 nanocomposite material the ZSM-5 structure was partially disrupted resulting in overall decrease of the Al^{IV} species in tetrahedral positions and formation of other types of Al coordination sites. The deconvolution of the spectrum shows that the broad resonance is best fitted with two components with chemical shifts at around 30 and 50 ppm. Previous studies showed that these resonances are associated with aluminum atoms in pentacoordinated and

Table 1
Textural properties of the parent, carboxilic-, and sulfonic-functionalized and verapamil loaded mesoporous ZSM-5/KIT-6 and ZSM-5/SBA-15 silica materials.

Samples	S_{BET} (m^2/g)	Pore volume (cm^3/g)	PD[a] (nm)	COOH/SO_3H/verapamil content (wt%)
ZSM-5/KIT-6	425	1.18	11.0	–
ZSM-5/SBA-15	362	1.20	12.0	–
ZSM-5/KIT-6-COOH	285.4	0.82	9.5	12.5
ZSM-5/SBA-15-COOH	282.1	1.04	11.6	11.3
ZSM-5/KIT-6-SO_3H	399.8	1.10	9.9	7.3
ZSM-5/SBA-15-SO_3H	351.5	1.31	14.6	4.0
Ver/ZSM-5/KIT-6-COOH	46.3	0.19	8.6	17.1
Ver/ZSM-5/SBA-15-COOH	66.4	0.34	11.6	21.3
Ver/ZSM-5/KIT-6-SO_3H	216.2	0.63	7.9	19.4
Ver/ZSM-5/SBA-15-SO_3H	46.0	0.23	12.0	33.6

distorted tetrahedral coordinated state, respectively [25,26]. These species are usually present in small amounts in zeolite materials, however literature data show that the hydrothermal procedure may result in their increase at the expense of the framework tetra-coordinated AlO_4 structural units (signal at 58 ppm) [25].

Based on ^{27}Al NMR spectra of the two materials we can conclude that the amount of framework Al species in tetrahedral coordination in ZSM-5/KIT-6 nanocomposite is much higher compared to ZSM-5/SBA-15 material.

In good accordance with solid state NMR spectra TEM images show the presence of small micrporous areas embedded in the mesoporous structure of SBA-15 and KIT-6 (Supplementary data, Fig. SD2).

Comparison of ^{27}Al spectra of the parent non-modified ZSM-5/KIT-6 (Supplementary data, Fig. SD1a) and ZSM-5/KIT-6-COOH materials (Supplementary data, Fig. SD1c) demonstrates that the two samples have identical spectral patterns indicating that the introduction of organic groups did not result in any significant changes in Al coordination type.

The modification with $-(CH_2)_3NHCO(CH_2)_2COOH$ groups was confirmed by $^1H \rightarrow {}^{13}C$ CP and $^1H \rightarrow {}^{29}Si$ CP NMR spectra. The $^1H \rightarrow {}^{13}C$ CP spectrum of the sample (Supplementary data, Fig. SD3) shows the characteristic resonances for the methylene groups (54, 42, 29, 21, 16 and 9 ppm) as well as a broad resonance at 177 ppm for the two carbonyl atoms from −CONH and −COOH functions. The presence of the resonances at −57 and −65 ppm in the $^1H \rightarrow {}^{29}Si$ CP spectrum which are typical respectively for the T^2 [(SiO)2Si-(R_1)-OR_2)] and T^3 [$(SiO)_3$Si-R1] structural units ($R_1 = (CH_2)_3NH_2NHCO(CH_2)_2COOH$; $R_2 = CH_2CH_3$) from the silica framework additionally confirms the successful functionalization of ZSM-5/KIT-6 with organic groups (Supplementary data, Fig. SD4).

The surface modification of silica carriers resulted in some decrease of low-angle [1 0 0] reflection intensity (Supplementary data, Fig. SD5), which is due to decreased 'scattering contrast' between silica wall and organic material filled pores compared to that of adsorbed water of parent silica [27]. Nitrogen adsorption and desorption isotherms of the parent, − $(CH_2)_3SO_3H$ and $-(CH_2)_3NHCO(CH_2)_2COOH$ modified ZSM-5/KIT-6 and ZSM-5/SBA-15 samples are presented in Fig. 3. The calculated textural parameters are summarized in Table 1. Parent ZSM-5/KIT-6 and ZSM-5/SBA-15 nanocomposites have a type IV isotherm with H1 hysteresis loop at high relative pressures. This type of isotherms is characteristic for mesoporous materials with pore size above 4 nm. The functionalization with − $(CH_2)_3SO_3H$ and − $(CH_2)_3NHCO(CH_2)_2COOH$ groups resulted in decreased surface area, pore volume and pore size, which is more pronounced for the COOH-modified the ZSM-5/SBA-15 and ZSM-5/KIT-6 samples. This can be explained by pore blocking and narrowing due to bounding of long chain of $-(CH_2)_3NHCO(CH_2)_2COOH$ functional groups on the wall surface of the silica carrier. Significant decrease of surface area and pore volume was also witnessed by verapamil loading indicating the penetration of the drug molecules into the channel system (Table 1). Higher-angle XRD patterns of verapamil loaded $-(CH_2)_3SO_3H$ and $-(CH_2)_3NHCO(CH_2)_2COOH$ modified ZSM-5/KIT-6 and ZSM-5/SBA-15 samples (Fig. 2) do not show any presence of crystalline verapamil. Despite the different drug loadings on the modified ZSM-5/KIT-6 and ZSM-5/SBA-15 samples it seems that the drug remaining on the external surface is in amorphous state.

3.3. FT-IR spectroscopic characterization of the modified and drug loaded materials

The ATR-FT-IR spectrum of pure verapamil (Fig. 4) corresponds to that found in the literature for racemic verapamil HCl with several overlapping bands around 1471 cm^{-1} [28]. Since the silica structure have very strong absorption of Si−O−Si stretching from 1200 to 900 cm^{-1}, only the spectral region of 1800–1300 cm^{-1} is discussed in details. In this region verapamil exhibits skeletal stretching vibrations of benzene rings at 1610, 1594 and at 1519 cm^{-1}. The bands at 1470,

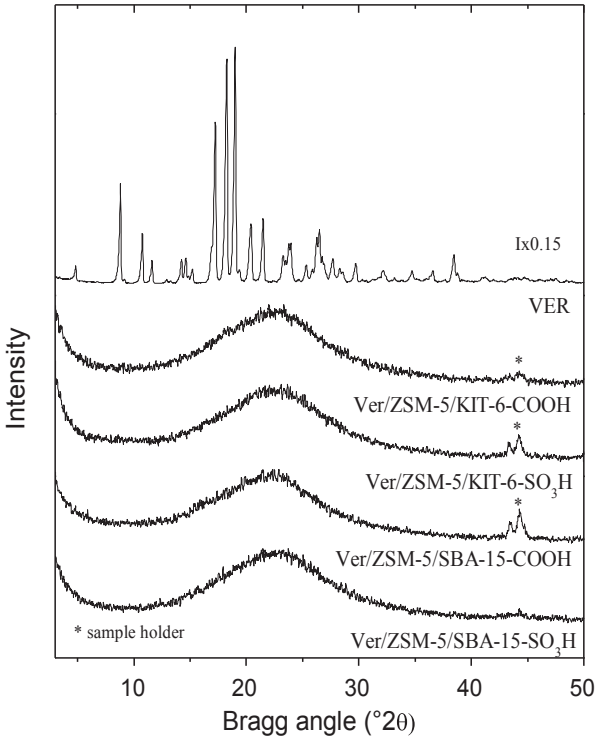

Fig. 2. XRD patterns of the initial and modified ZSM-5/SBA-15 and ZSM-5/KIT-6 materials and verapamil loaded formulations.

1462, 1448 and 1417 cm^{-1} belong mainly to aromatic C−H and CH_2 deformations. The bands from 1400 to 1300 cm^{-1} might belong to CCC_{ring} and CN deformations [15].

In the spectra of $-(CH_2)_3NHCO(CH_2)_2COOH$-modified materials (Fig. 4), the strong C=O stretching band at 1724 cm^{-1} suggests that the −COOH is in protonated form or the verapamil interact with the silica surface through the −C−O− of the carboxyl groups. Another change in the spectra is that the multiple bands around 1471 cm^{-1} are supressed and new bands at 1465, 1455 and 1444 cm^{-1} arise. It seems plausible that a sterically hindrance of the verapamil molecules exists due to its entering in the pores of the ZSM-5/SBA-15-COOH and ZSM-5/KIT-6-COOH. Similar tendency was observed also for $-(CH_2)_3SO_3H$-containing ZSM-5/SBA-15 and ZSM-5/KIT-6 materials due to the stronger interaction with more acidic functional groups. In this latter case, however, some shift in the skeletal ring stretching (νC=C) at 1606 and 1592 cm^{-1} occurs as well (Fig. 4).

3.4. Modeling of the interactions of verapamil with −COOH and $-SO_3H$ groups on the modified silica matrix

(a) Interaction of verapamil with $-(CH_2)_3SO_3H$ and $-(CH_2)_3NHCO(CH_2)_2COOH$

We have performed density functional study on the interaction of verapamil molecule with acetic acid (CH_3COOH) and methane sulfonic acid (CH_3SO_3H) as a model system of the interaction of verapamil with $-(CH_2)_3SO_3H$ and $-(CH_2)_3NHCO(CH_2)_2COOH$ functionalized silica matrices. In both cases three types of complexes were considered with coordination of the −COOH or $-SO_3H$ groups to the methoxy group, tertiary amino group, and −C≡N group in verapamil molecule. In this way we can estimate the strength of the interaction of the $-(CH_2)_3SO_3H$ and $-(CH_2)_3NHCO(CH_2)_2COOH$ fragments with the three most plausible coordination sites in verapamil molecule.

(b) Interaction of verapamil with CH_3COOH

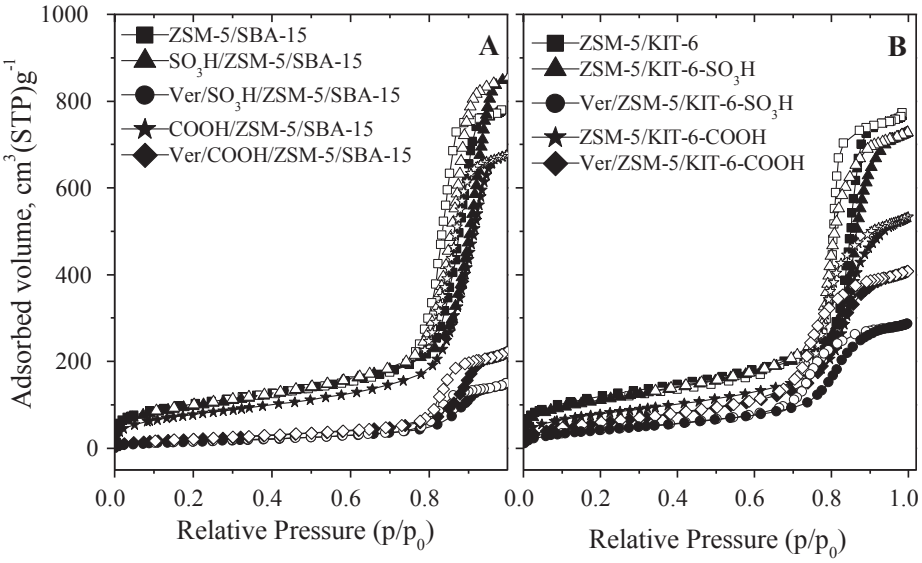

Fig. 3. Nitrogen adsorption and desorption isotherms of the initial and modified ZSM-5/SBA-15 and ZSM-5/KIT-6 materials and verapamil loaded formulations.

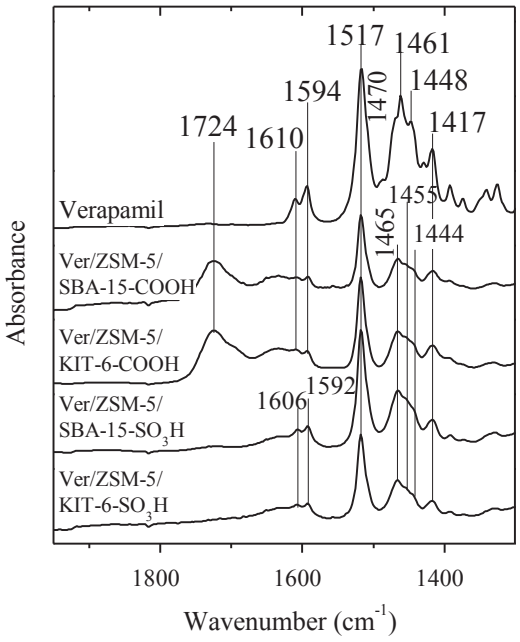

Fig. 4. ATR FT-IR spectra of the initial and modified ZSM-5/SBA-15 and ZSM-5/KIT-6 materials and verapamil loaded formulations.

Interaction of verapamil with CH_3COOH leads to formation of H-bonded complexes with different stability. The coordination of the −COOH group to the methoxy or −CN group in verapamil leads to very similar binding energies, –32 and −29 kJ/mol, respectively, while the strongest interaction was found for the coordination of the −COOH group to the tertiary amino group in verapamil, with almost twice higher binding energy as absolute value, −61 kJ/mol. In the three studied complexes an H-bond between −COOH group as a proton donor and methoxy, amino, or −CN group in verapamil as a proton acceptor is formed (Fig. 5). In accordance with the BE values, the H-bond length in the three studied complexes ranges from 1.53 Å in the most stable one (Fig. 5c) to 1.87 and 1.98 Å in the complexes with −CN and methoxy groups respectively.

In addition to the stability of the complexes of verapamil with acetic acid we have calculated their vibrational frequencies (Fig. 6). First, we will compare the vibrational frequencies of verapamil molecule in gas phase with the available experimental data. According to the experimental data the skeletal stretching vibrations in the verapamil are at 1610, 1594, and 1519 cm^{-1}. We have found that the corresponding scaled calculated frequencies for skeletal stretching at 1616, 1607, 1594, 1588, and 1500 cm^{-1} are in very good agreement with the experimental ones. We also found very good agreement between experimental and scaled calculated frequencies for the aromatic C−H and CH_2 deformations, and CCC_{ring} and CN deformations as well. The degrees of freedom which can be used for monitoring the interaction between −COOH group and the three functional groups in verapamil are the C═O and O−H stretching vibrations in the −COOH group. We have calculated the scaled value for the C═O stretching vibration in −COOH group coordinated to the −CN, methoxy, and amino group in the verapamil to be 1726, 1728, and 1663 cm^{-1}, respectively. If we compare these values with the experimental one, which is at 1724 cm^{-1}, we may conclude that most likely in the experiment the −COOH group is coordinated to −CN or methoxy group. Since they have very similar energies of formation we cannot designate them. Interestingly, the most stable complex of −COOH group is with the tertiary amino group, but this complex is showing stronger shift in C═O stretching vibration by ~70 cm^{-1}. One possible explanation for the lack of formation of this

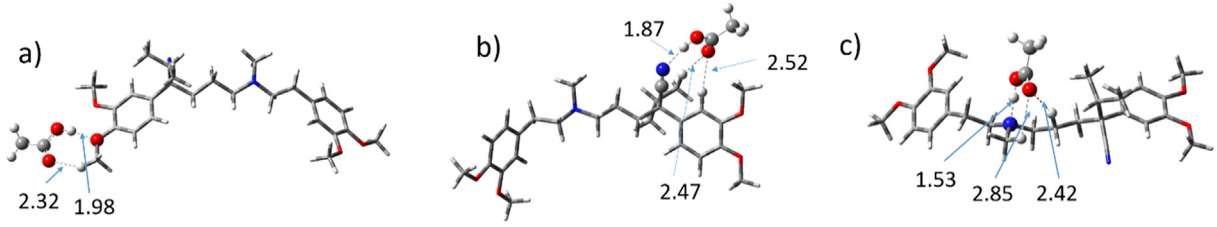

Fig. 5. Complexes of $-(CH_2)_3NHCO(CH_2)_2COOH$ with (a) methoxy, (b) tertiary amino, and (c) nitrile group in verapamil. Selected distances are shown in Å.

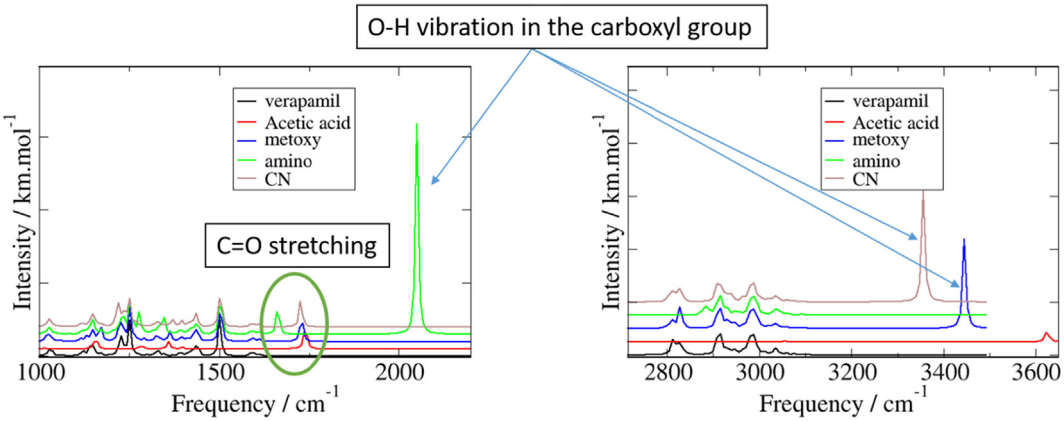

Fig. 6. Scaled calculated IR frequencies in the three modeled complexes of verapamil with acetic acid.

complex may be the steric hindrance, since the tertiary amino group is in the middle of the verapamil molecule and is not so accessible for the functionalized silica support.

The stretching O−H vibration of the −COOH group is also shifted to lower frequencies due to the formation of hydrogen bond with the verapamil molecule and the red shift is proportional to the strength of the interaction.

(c) Interaction of verapamil with -$(CH_2)_3SO_3H$

The interaction of the − $(CH_2)_3SO_3H$ group with verapamil is somewhat stronger in comparison with − $(CH_2)_3NHCO(CH_2)_2COOH$ (Table 2). The binding energy of the complexes with −CN, and methoxy group in verapamil is −20 and −50 kJ/mol, respectively. Again the strongest interaction was found with the tertiary amino group, −103 kJ/mol. The interaction with this amino group leads to deprotonation of the -SO_3H group and its proton is transferred to the N atom from the amino group in verapamil. Thus, an ammonium cation is formed and the $-SO_3^-$ anion interacts with this cation electrostatically and via hydrogen bond (Fig. 7c).

There are no disdinguishable changes in the calculated IR spectra for the complexes of $-(CH_2)_3SO_3H$ with methoxy, tertiary amino, and nitrile group in verapamil in comparison to the verapamil complexes with carboxilic group. In contrast to the coordination of verapamil to the −COOH group, here the vibrations of the $-SO_3H$ group are bellow 1300 cm^{-1} (at 1250 cm^{-1} the O═S═O vibrations) and overlap with the sceletal vibrations of verapamil (Supplementary data, Fig. SD6).

3.5. Polymer coating and in vitro release measurements

The nanocomposite particles contain surface acid groups, − $(CH_2)_3SO_3H$ or − $(CH_2)_3NHCO(CH_2)_2COOH$ groups, therefore the first polymer layer deposited on the nanoparticles is favorably made of chitosan. To obtain the next shell layer an opositely charged κ-carrageenan was used forming a polyelectrolyte complex with the chitosan. Polysulfobetaine chain grafted chitosan was applied for the formation of the third layer around the carrier nanoparticles. It is well known that polyzwitteriones are characterized with extremely good biocompatibility and low unspecific protein adsorption, making them suitable materials for biological applications [29–31]. Therefore, polysulfobetaine with an average molar mass number Mn = 10,000 g/mol and end cyclic carbonate functionality was first synthesed and used for chitosan modification. The PSB chains were grafted on chitosan via selective reaction of the cyclic carbonate moieties with the amino groups of the polysaccharide.

Table 2
Binding energies (in kJ/mol) of acetic acid (CH_3COOH) and methane sulfonic acid (CH_3SO_3H) with the three most plausible coordination sites in verapamil molecule (methoxy, tertiary amino, and nitril groups).

Group	CH_3COOH	CH_3SO_3H
methoxy	−832	−50
CN	−29	−20
amino	−61	−103

The TG analysis data show successful polymer coating around the particles which is in the range of 22.7–25.0 wt% i.e. 23.7 wt%, for Ver/ZSM-5/KIT-6-COOH/P; 22.9 wt%, for Ver/ZSM-5/SBA-15-COOH/P; 24.6 wt% and for Ver/ZSM-5/SBA-15-SO_3H/P; 24.9 wt% for Ver/ZSM-5/KIT-6-SO_3H/P.

Atomic force microscopy (AFM) was used for visualization of the modified ZSM-5/KIT-6-SO_3H carrier prior and after polymer coating of the drug loaded particles. Fig. 8 displays the AFM images of the spin-coated nanoporous particles on glass wafers. ZSM-5/KIT-6-SO_3H material presents quite uniform and spherical particles (Fig. 8, left image). Their dimensions measured in the horizontal distance varied from 63 nm to 86 nm with an average value of 78 ± 7 nm calculated from the long and short cross-sections of 15 particles (See also Supplementary data, Fig. SD7). Upon coating the particles size was increased as visualized in Fig. 8, the right image. The average size of Ver/ZSM-5/KIT-6-SO_3H/P particles calculated for 15 species is 136 ± 13 nm. This is also evidenced from the cross-section curves of two particles from the corresponding AFM image (Supplementary data, Fig. SD8). The right image in Fig. 8 displays also a polymer film formed on the wafer surface which could be attributed to partial dissolution of the third layer of grafted chitosan during particles dispersion in aqueous medium due to increased solubility of the grafted with PSB chitosan.

Particle size distribution was measured for the polymer coated and drug loaded Ver/ZSM-5/KIT-6-SO_3H/P particles applying dynamic light scattering (DLS) technique. Particles were dispersed in an aqueous medium with a concentration of 1 mg/ml and DLS measurement performed at 25 °C and scattering angle θ = 90°. Fig. 9 displays the distribution curve of the hydrodynamic size ($D_h^{90°}$) of the polymer coated particles. A single population of particles with size in the range from 145 nm to 370 nm (a mean $D_h^{90°}$ = 238 nm) was observed. The size distribution of the particles was considerably narrower as indicated by dispersity index values varying between 0.20 and 0.26 obtained for five consecutive measurements. The nanocolloidal solution of the polymer coated particles was stable over time. DLS measurements performed after 2 days displayed similar particle size and distribution ranges. On the contrarary, a trend toward increasing the particles size was observed during the DLS experiment of the drug loaded Ver/ZSM-5/KIT-6-SO_3H particles without polymer coating. Immediately after sonication of their aqueous dispersion, particles with size of about 200 nm were detected and then over the course of several minites the size doubled. It

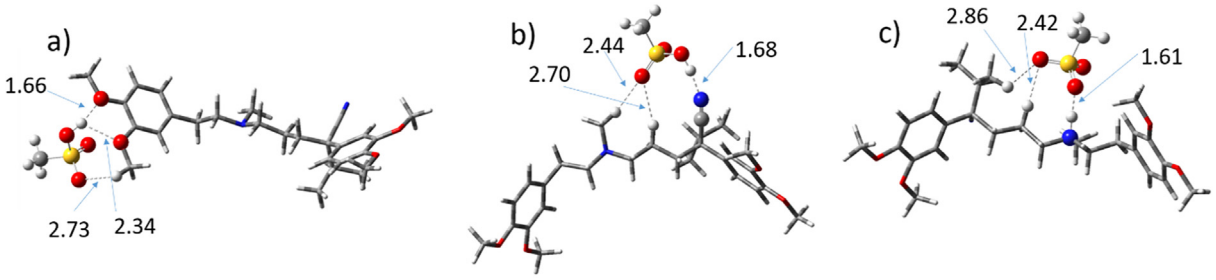

Fig. 7. Complexes of $-CH_3(CH_2)_2SO_3H$ with (a) methoxy, (b) tertiary amino, and (c) nitrile group in verapamil. Selected distances are shown in Å.

was an indication of aggregation of the uncoated particles in an aqueous medium, as well as proof that polymer coating was a key step for improving the stability of the colloidal system.

3.6. In vitro release of verapamil

In-vitro release study of verapamil was carried out in phosphate buffered saline at pH 7.4, relevant to the physiological pH of the blood. As evident from the results shown in Fig. 10, non coated mesoporous nanocomposites are characterized with initial burst release of verapamil, whereas the total drug release was observed in 60 min for all samples. The high verapamil dispersion in the pore system of ZSM-5/KIT-6 modified by $-SO_3H$ or $-COOH$ groups can be a reason for its slower release from this type carrier in comparison to the ZSM-5/SBA-15 analogues.

The polymers coating of particles was associated with decrease in release rate, and this effect was most pronounced for ZSM-5/KIT-6 based formulation, especially for its ZSM-5/KIT-6-SO_3H counterpart. This effect can be associated with the smaller pore size and 3D structure of the ZSM-5/KIT-6 carrier and the presence of polymer coating around the particles, which acts as a diffusion controlling barrier, together with strong adsorption sites.

Faster drug release was encountered from uncoated nanocomposite silicas and this tendency was more pronounced for the formulations prepared on ZSM-5/SBA-15 as compared to their ZSM-5/KIT-6 analogues (Fig. 10). Total verapamil release was achieved in 2 h for all studied samples. The modification by $-(CH_2)_3SO_3H$ groups lead to slower release, most probably because of the stronger interaction of verapamil with stronger acidic groups. As could be expected, coating with a polymer complex resulted in a decrease of verapamil release, fitting to the formerly observed release trend. Thus, the deposition of multilayer polymer coating is a feasible approach for improved verapamil release.

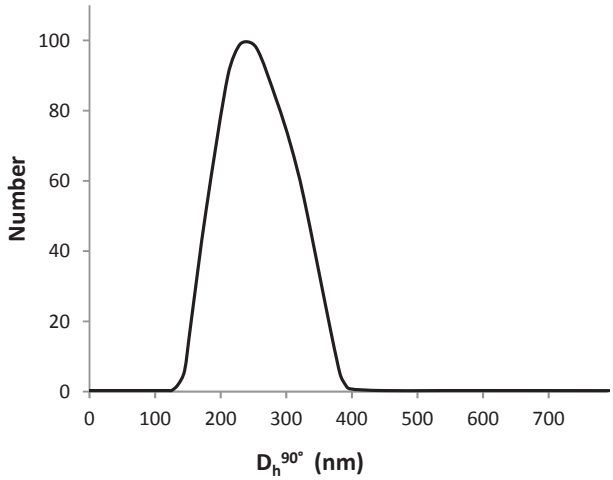

Fig. 9. The distribution of the hydrodynamic diameter of the drug loaded and polymer coated Ver/ZSM-5/KIT-6-SO_3H/P particles in an aqueous medium with concentration 1 mg/ml, measured at 25 °C and at scattering angle θ = 90°.

3.7. CTM

Summarized data obtained by the Chou-Talalay methodology are presented in Tables 3–11 according to cell line. For the referent 1:1 dose ratio combination of doxorubicin and verapamil are generated CI and DRI indices both for the actual viability data points (Tables 3, 6, 9) and for each dataset of the simulated "dose-response" curve (Tables 4, 7, 10). In the non-constant ratio experiment with Dox and the verapamil formulations S1/2/3/4 are given only CI and DRI parameters yielded at actual experimental points (Tables 5, 8, 11).

A quick overview of the Compusyn® report shows well defined trends in the synergistic behaviour of verapamil based on its formulation. Irrelevant of tumor cell type, free verapamil achieves strongest

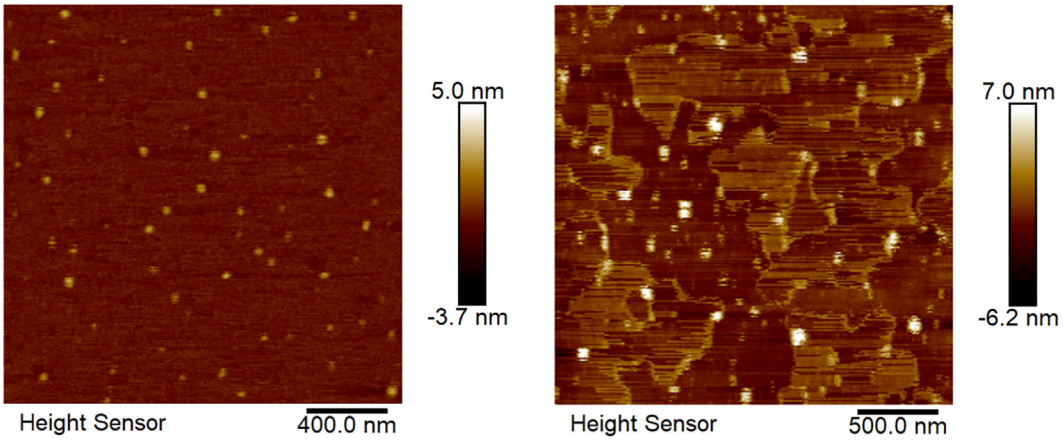

Fig. 8. AFM images of the ZSM-5/KIT-6SO_3H (left) and verapamil loaded and polymer coated Ver/ZSM-5/KIT-6-SO_3H/P (right) particles.

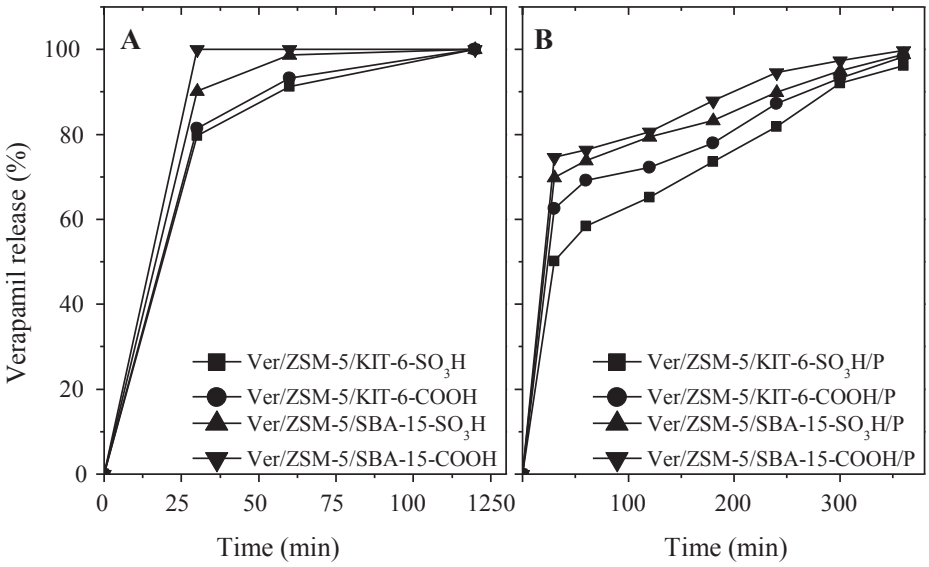

Fig. 10. Release profiles of verapamil loaded SO_3H or COOH modified ZSM-5/SBA-15 and ZSM-5/KIT-6 carriers (A) and their polymer coated analogues (B).

Table 3
Growth inhibitory effects on HL-60 cells (as fraction affected, Fa) of both drugs Dox and Ver alone and in a fixed 1:1 ratio combination at actual experimental points. CI values < 1 and DRI estimates > 1 that are indicative of a synergistic drug interaction are highlighted in bold italic.

Dox and Ver single drug effects				*Dox + Ver 1:1 fixed dose combination*			
Dose Dox [μM]	Fa	Dose Ver [μM]	Fa	Total dose [μM]	Fa	CI	DRI Dox
40.0	0.89	40.0	0.32	80.0	0.84	***1.15802***	***0.87110***
20.0	0.75	20.0	0.29	40.0	0.71	***0.82709***	***1.24426***
10.0	0.11	10.0	0.24	20.0	0.71	***0.41355***	***2.48851***
5.0	0.03	5.0	0.16	10.0	0.64	***0.24255***	***4.32158***
2.5	0.03	2.5	0.11	5.0	0.58	***0.13862***	***7.73156***

Table 4
CI and DRI estimates for data points of the simulated "dose-response" curve in the constant 1:1 ratio experiment on HL-60 cells. CI values < 1 and DRI estimates > 1 that indicate synergistic cytotoxic activity are highlighted in bold italic.

Fa	Dose Dox alone [μM] that produces Fa	Total dose [μM] that produces Fa	CI	DRI Dox
0.05	4.57183	0.00290	***0.00423***	***3152.51***
0.10	6.35746	0.01639	***0.00619***	***775.883***
0.15	7.79721	0.04788	***0.00870***	***325.711***
0.20	9.09259	0.10732	***0.01216***	***169.441***
0.25	10.3233	0.20905	***0.01695***	***98.7650***
0.30	11.5340	0.37427	***0.02358***	***61.6342***
0.35	12.7562	0.63522	***0.03278***	***40.1631***
0.40	14.0168	1.04203	***0.04557***	***26.9029***
0.45	15.3425	1.67495	***0.06352***	***18.3199***
0.50	15.7630	2.66669	***0.08903***	***12.5722***
0.55	18.3150	4.24564	***0.12599***	***8.62770***
0.60	20.0472	6.82439	***0.18093***	***5.87517***
0.65	22.0284	11.1949	***0.26554***	***3.93543***
0.70	24.3627	19.0002	***0.40219***	***2.56447***
0.75	27.2199	34.0173	***0.63807***	***1.60035***
0.80	30.9041	66.2590	***1.08641***	***0.93283***
0.85	36.0383	148.528	***2.07668***	***0.48527***
0.90	44.1998	433.938	***4.92719***	***0.20372***
0.95	61.4630	2451.78	***19.9681***	***0.05014***
0.97	77.7140	8405.90	***54.1092***	***0.01849***

Table 5
Experimental datasets for the non-fixed combination treatments with Dox and S1/2/3/4in HL-60 cells.

	Dose Dox [μM]	Dose S1[μM] (respective Ver dose)	Fa	Dose Dox [μM] alone that produces Fa	CI	DRI Dox
S1	15.0	10.0	0.91	46.5295	***0.35280***	***3.10197***
	15.0	5.0	0.91	46.5295	***0.33759***	***3.10197***
	15.0	2.0	0.89	42.1710	***0.36318***	***2.81140***
	15.0	1.0	0.72	25.4299	***0.60075***	***1.69533***
	15.0	0.5	0.49	15.4697	***0.92440***	***1.09798***
	Dose Dox [μM]	Dose S2 [μM] (respective Ver dose)	Fa	Dose Dox [μM] alone that produces Fa	CI	DRI Dox
S2	15.0	10.0	0.90	44.1998	***0.34708***	***2.94665***
	15.0	5.0	0.90	44.1998	***0.34323***	***2.94665***
	15.0	2.0	0.89	42.1710	***0.35744***	***2.81140***
	15.0	1.0	0.69	23.8607	***0.63268***	***1.59072***
	15.0	0.5	0.47	15.8975	***0.94955***	***1.05983***
	Dose Dox [μM]	Dose S3 [μM] (respective Ver dose)	Fa	Dose Dox [μM] alone that produces Fa	CI	DRI Dox
S3	15.0	10.0	0.91	46.5295	***0.33000***	***3.10197***
	15.0	5.0	0.9	44.1998	***0.34371***	***2.94665***
	15.0	2.0	0.89	42.1710	***0.35765***	***2.81140***
	15.0	1.0	0.51	17.0616	***0.88896***	***1.13744***
	15.0	0.5	0.46	15.6180	***0.96656***	***1.04120***
	Dose Dox [μM]	Dose S4 [μM] (respective Ver dose)	Fa	Dose Dox [μM] alone that produces Fa	CI	DRI Dox
S4	15.0	10.0	0.9	44.1998	***0.34049***	***2.94665***
	15.0	5.0	0.83	33.7455	***0.44590***	***2.24970***
	15.0	2.0	0.72	25.4299	***0.59130***	***1.69533***
	15.0	1.0	0.69	23.8607	***0.62954***	***1.59072***
	15.0	0.5	0.45	15.0126	***0.99956***	***1.00684***

synergistic effects (CI < < < 1) with Dox at the lowest Fa values that correspond to negligible cytostatic activity. In the chemosensitive HL-60 cell line both experimental and simulated data (Tables 3 and 4) show that synergism is much less pronounced beyond the point of Fa = 0.5, whereby the same combination abruptly turns antagonistic at Fa values higher than 0.8 that are actually aimed. A similar synergy profile of the drug duo was established in the HT-29 cell line (Tables 9, 10), whereas

Table 6
Growth inhibitory effects on HL-60/Dox cells (as fraction affected, Fa) of both drugs Dox and Ver alone and in a fixed 1:1 ratio combination at actual experimental points. CI values < 1 and DRI estimates > 1 that are indicative of a synergistic drug interaction are highlighted in bold italic.

Dox and Ver single drug effects				*Dox + Ver 1:1 fixed dose combination*			
Dose Dox [μM]	Fa	Dose Ver [μM]	Fa	Total dose [μM]	Fa	CI	DRI Dox
40.0	0.55	40.0	0.29	80.0	0.78	***0.33838***	***3.23163***
20.0	0.48	20.0	0.26	40.0	0.74	***0.22118***	***5.00688***
10.0	0.24	10.0	0.23	20.0	0.69	***0.14957***	***7.52514***
5.0	0.16	5.0	0.14	10.0	0.58	***0.13535***	***8.64215***
2.5	0.12	2.5	0.08	5.0	0.31	***0.28697***	***4.68721***

Table 7
CI and DRI estimates for data points of the simulated "dose-response" curve in the constant 1:1 ratio experiment on HL-60/Dox cells. CI values < 1 and DRI estimates > 1 that indicate synergistic cytotoxic activity are highlighted in bold italic.

Fa	Dose Dox [μM] alone that produces Fa	Total dose [μM] that produces Fa	CI	DRI Dox
0.05	0.96959	0.14079	***0.16977***	***13.7738***
0.10	2.31056	0.40916	***0.16243***	***11.2942***
0.15	3.95558	0.79205	***0.16249***	***9.98825***
0.20	5.92931	1.30234	***0.16472***	***9.10562***
0.25	8.28326	1.96385	***0.16795***	***8.43573***
0.30	11.0928	2.81152	***0.17178***	***7.89099***
0.35	14.4626	3.89473	***0.17609***	***7.42677***
0.40	18.5371	5.28334	***0.18083***	***7.01717***
0.45	23.5182	7.07776	***0.18603***	***6.64565***
0.50	29.6951	9.42597	***0.19174***	***6.30069***
0.55	37.4943	12.5532	***0.19809***	***5.97364***
0.60	47.5694	16.8168	***0.20523***	***5.65737***
0.65	60.9707	22.8126	***0.21341***	***5.34536***
0.70	79.4925	31.6017	***0.22299***	***5.03089***
0.75	106.455	45.2422	***0.23458***	***4.70602***
0.80	148.718	68.2224	***0.24924***	***4.35981***
0.85	222.925	112.176	***0.26909***	***3.97454***
0.90	381.637	217.151	***0.29926***	***3.51495***
0.95	909.451	631.084	***0.35819***	***2.88219***
0.97	1687.00	1348.20	***0.40883***	***2.50259***

a more consistent synergistic behaviour was found in the HL-60/Dox strain (Tables 6, 7).

Interestingly, a nearly reciprocal synergistic pattern was observed in the varying-ratio experiment with Dox and the verapamil-loaded nanocomposites S1/2/3/4. The four verapamil-delivery systems behave very much alike both between and within cell lines, whereby the boosting effect of the released P-gp inhibitor escalates as the Fa grows.

In the HL-60 experiment treating cells with a half-inhibitory concentration of Dox (15 μM) produced a superadditive effect in the presence of S1/2/3/4-released verapamil in micromolar concentrations as low as 1.0 μM. Estimated Fa values in the 10.0–1.0 μM verapamil concentration range are well above 0.5 (growth inhibitory effect of 15 μM Dox) and DRI indices imply a nearly 3-fold reduction in the equi-effective dose of doxorubicin when combined with S1/2/3/4 portions respective to 10, 5, 2 μM of the efflux pump inhibitor. The lowest verapamil aliquot of 0.5 μM delivered not less than an additive effect with CI and DRI estimates ranging near 1.

In the multi-drug resistant HL-60/Dox variant a similar response pattern to the S1/2/3/4 cargo was observed. However, combinations of doxorubicin in half-maximal inhibitory concentrations (30 μM) with S1/2/3/4-carried verapamil aliquots in the 10.0–2.0 μM concentration range resulted in a much stronger synergistic effect with a 5–8-fold reduction of the equi-effective Dox dose (DRI indices). Minimal quantities of the S1/2/3/4 drug load (0.5 μM verapamil), on the other hand, exerted modest antagonism in the tested ratio combination with

Table 8
Experimental datasets for the non-fixed combination treatments with Dox and S1/2/3/4 in HL-60/Dox cells.

	Dose Dox [μM]	Dose S1 [μM] (respective Ver dose)	Fa	Dose Dox [μM] alone that produces Fa	CI	DRI Dox
S1	30.0	10.0	0.85	222.925	***0.13955***	***7.43084***
	30.0	5.0	0.84	203.992	***0.14981***	***6.79972***
	30.0	2.0	0.82	172.983	***0.17474***	***5.76610***
	30.0	1.0	0.59	45.3296	***0.66468***	***1.51099***
	30.0	0.5	0.35	14.4626	***2.07933***	***0.48209***
	Dose Dox [μM]	Dose S2[μM] (respective Ver dose)	Fa	Dose Dox [μM] alone that produces Fa	CI	DRI Dox
S2	30.0	10.0	0.86	244.841	***0.30085***	***8.16136***
	30.0	5.0	0.86	244.841	***0.21169***	***8.16136***
	30.0	2.0	0.83	187.487	***0.20161***	***6.24955***
	30.0	1.0	0.61	49.9400	***0.64530***	***1.66467***
	30.0	0.5	0.41	19.4530	***1.58056***	***0.64843***
	Dose Dox [μM]	Dose S3[μM] (respective Ver dose)	Fa	Dose Dox [μM] alone that produces Fa	CI	DRI Dox
S3	30.0	10.0	0.86	244.841	***0.12275***	***8.16136***
	30.0	5.0	0.85	222.925	***0.13470***	***7.43084***
	30.0	2.0	0.83	187.487	***0.16008***	***6.24955***
	30.0	1.0	0.59	45.3296	***0.66213***	***1.51099***
	30.0	0.5	0.42	20.4069	***1.47063***	***0.68023***
	Dose Dox [μM]	Dose S4[μM] (respective Ver dose)	Fa	Dose Dox [μM] alone that produces Fa	CI	DRI Dox
S4	30.0	10.0	0.85	222.925	***0.13457***	***7.43084***
	30.0	5.0	0.84	203.992	***0.14706***	***6.79972***
	30.0	2.0	0.84	203.992	***0.14706***	***6.79972***
	30.0	1.0	0.61	49.9400	***0.60072***	***1.66467***
	30.0	0.5	0.33	13.0393	***2.30075***	***0.43464***

Table 9
Growth inhibitory effects on HL-60/Dox cells (as fraction affected, Fa) of both drugs Dox and Ver alone and in a fixed 1:1 ratio combination at actual experimental points. CI values < 1 and DRI estimates > 1 that are indicative of a synergistic drug interaction are highlighted in bold italic.

Dox and Ver single drug effects				*Dox + Ver 1:1 fixed dose combination*			
Dose Dox [μM]	Fa	Dose Ver [μM]	Fa	Total dose [μM]	Fa	CI	DRI Dox
40.0	0.61	40.0	0.41	80.0	0.7	***0.91325***	***2.10245***
20.0	0.34	20.0	0.29	40.0	0.64	***0.60779***	***2.98170***
10.0	0.35	10.0	0.13	20.0	0.6	***0.36405***	***4.81083***
5.0	0.19	5.0	0.08	10.0	0.55	***0.22675***	***7.42708***
2.5	0.13	2.5	0.02	5.0	0.21	***0.62056***	***2.15923***

calculated CI indices > 1. However, a cellular response to verapamil in a slightly reversed dose-dependent manner is not uncommon, as many studies report a stimulated P-gp ATP-ase activity by low concentrations of the drug [17,32].

The strongest and most consistent synergistic response to the non-fixed ratio combinations of Dox and S1/2/3/4 was observed in the MDR-1 overexpressing HT-29 cell line (Table 11). CI values calculated at all actual experimental data points are strictly < 1 even at the lowest S1/2/3/4 co-treatment equivalent to 0.5 μM verapamil. A slightly better performance was obtained using S3/4 as verapamil carriers by which DRI indices suggest a nearly 10-fold reduction of the 30 μM IC50 value of Dox (3:1 and 6:1 ratio experiments). However, in the same dose ratio combinations, both S1 and S2 polymers delivered closely comparable total inhibitory effects of ca. 84% (Fa = 0.84).

The major advantages of nanoparticulate drug delivery systems,

Table 10
CI and DRI estimates for data points of the simulated "dose-response" curve in the constant 1:1 ratio experiment on HT-29 cells. CI values < 1 and DRI estimates > 1 that indicate synergistic cytotoxic activity are highlighted in bold italic.

Fa	Dose Dox [μM] alone that produces Fa	Total dose [μM] that produces Fa	CI	DRI Dox
0.05	0.69683	0.21528	***0.17946***	***6.47381***
0.10	1.79204	0.64512	***0.22102***	***5.55569***
0.15	3.21608	1.27275	***0.25362***	***5.05375***
0.20	4.99513	2.12288	***0.28273***	***4.70599***
0.25	7.18595	3.23918	***0.31037***	***4.43689***
0.30	9.87314	4.68540	***0.33768***	***4.21442***
0.35	13.1756	6.55166	***0.36544***	***4.02205***
0.40	17.2592	8.96579	***0.39432***	***3.85001***
0.45	22.3590	12.1123	***0.42501***	***3.69196***
0.50	28.8151	16.2641	***0.45830***	***3.54339***
0.55	37.1354	21.8392	***0.49520***	***3.40080***
0.60	48.1083	29.5035	***0.53704***	***3.26119***
0.65	63.0191	40.3749	***0.58579***	***3.12170***
0.70	84.0980	56.4567	***0.64449***	***2.97920***
0.75	115.547	81.6633	***0.71821***	***2.82983***
0.80	166.224	124.605	***0.81631***	***2.66801***
0.85	258.175	207.835	***0.95871***	***2.48442***
0.90	463.333	410.036	***1.19837***	***2.25996***
0.95	1191.55	1228.75	***1.75619***	***1.93945***
0.97	2333.42	2682.91	***2.33981***	***1.73947***

Table 11
Experimental data points for the non-fixed combination treatments with Dox + S1/2/3/4 [μM] on HT-29 cells.

	Dose Dox [μM]	Dose S1 [μM] (respective Ver dose)	Fa	Dose Dox [μM] alone that produces Fa	CI	DRI Dox
S1	30.0	10.0	0.84	234.415	***0.12823***	***7.81383***
	30.0	5.0	0.81	180.166	***0.16670***	***6.00555***
	30.0	2.0	0.8	166.224	***0.18056***	***5.54080***
	30.0	1.0	0.79	153.816	***0.19508***	***5.12721***
	30.0	0.5	0.56	39.0857	***0.76770***	***1.30286***
	Dose Dox [μM]	Dose S2[μM] (respective Ver dose)	Fa	Dose Dox [μM] alone that produces Fa	CI	DRI Dox
S2	30.0	10.0	0.84	234.415	***0.12805***	***7.81383***
	30.0	5.0	0.85	258.175	***0.11623***	***8.60582***
	30.0	2.0	0.82	195.926	***0.15314***	***6.53088***
	30.0	1.0	0.81	180.166	***0.16652***	***6.00555***
	30.0	0.5	0.55	37.1354	***0.80793***	***1.23785***
	Dose Dox [μM]	Dose S3 [μM] (respective Ver dose)	Fa	Dose Dox [μM] alone that produces Fa	CI	DRI Dox
S3	30.0	10.0	0.86	285.898	***0.10510***	***9.52995***
	30.0	5.0	0.85	258.175	***0.11630***	***8.60582***
	30.0	2.0	0.82	195.926	***0.15318***	***6.53088***
	30.0	1.0	0.8	166.224	***0.18052***	***5.54080***
	30.0	0.5	0.55	37.1354	***0.80805***	***1.23785***
	Dose Dox [μM]	Dose S4 [μM] (respective Ver dose)	Fa	Dose Dox [μM] alone that produces Fa	CI	DRI Dox
S4	30.0	10.0	0.86	285.898	***0.10783***	***9.52995***
	30.0	5.0	0.86	285.898	***0.10638***	***9.52995***
	30.0	2.0	0.85	258.175	***0.11685***	***8.60582***
	30.0	1.0	0.82	195.926	***0.15355***	***6.53088***
	30.0	0.5	0.52	31.8833	***0.94239***	***1.06278***

when applied in the systemic circulation, is their ability to accumulate predominantly into the tumor tissue due to EPR-effect and thus to deliver their cargo at high concentration into the target site, thus minimizing the side effects of the loaded drug for the healthy tissues. On this ground we prepared verapamil loaded nanocomposites in order to achieve passive targeting of the elaborated systems into the tumors and thus to assure high concentration of the drug at the site of action and to utilize its chemosensitizing properties by evading its inherent pharmacological effects as L-type calcium channel blocker. The obtained results of simultaneous treatment of cancer cells with verapamil loaded nanocomposites and free doxorubicin are promising, and they can establish the development of a dual drug delivery system for the simultaneous release of verapamil and doxorubicin.

4. Conclusions

Mesoporous ZSM-5/SBA-15 and ZSM-5/KIT-6 nanoparticles were synthesized and modified by post-synthesis method with $-(CH_2)_3SO_3H$ and $-(CH_2)_3NHCO(CH_2)_2COOH$ groups. Verapamil was loaded by incipient wetness impregnation on the functionalized composite supports. The drug loaded systems were further modified by surface coating with polymer complex layers composed of chitosan-κ-carrageenan-chitosan with grafted polysulfobetaine chains. ATR-FT-IR spectroscopic data suggested weak interaction of verapamil with the functional groups of the modified supports. Quantum-chemical calculations also proposed that verapamil binds weakly to the $-SO_3H$ and −COOH functional groups. The complexes are formed *via* a hydrogen bond between $-SO_3H$ or −COOH functional groups of the matrix and −CN or methoxy group of the verapamil molecule with binding energies of −20 to −50 kJ/mol. Complexes with the tertiary amino groups were found to be with higher binding energies, but the calculated IR frequencies in these cases do not fit to the experimental bands. Hence, such complexes should not be formed experimentally, most probably due to a steric hindrance.

The *in vitro* release profiles of verapamil from the composite carriers were investigated as a function of time showing modified release of verapamil for a period of 24 h. The factors influencing the verapamil delivery are the structure of the applied carrier, the chemical nature of functional groups and the presence of polymer complex around the composite nanoparticles. The bimodal pore structure of the ZSM-5/KIT-6 materials has positive effect on the verapamil release rate, independently of the nature of surface functional groups. Moreover, the ZSM-5/KIT-6 systems modified with stronger acidic $-(CH_2)_3SO_3H$ groups are characterized with slower drug release in line with our DFT calculations, which also found that verapamil binds stronger to the $-SO_3H$ groups compared to the −COOH groups. Additionally, the presence of polymer complex layers further deceased the drug release rate.

Based on the CTM comparative study on the MDR reversing capacity of free and nanoformulated verapamil, it can be concluded that loading of the drug into mesoporous nanocomposites drastically augments the antitumor efficacy of doxorubicin the high Fa-region of the "dose-response curve" as opposed to free drug. Moreover, synergistic effects are most pronounced in the MDR positive cellular models HT-29 and HL-60/Dox that overexpress the MDR-1 and MRP-1efflux pumps, respectively. Both membrane transporters appear to be equally well inhibited by extendedly released verapamil in the higher tested concentrations (10.0 μM, 5 μM and 2 μM), whereas the boosting effect of the lower micromolar doses (1.0 μM and 0.5 μM) was more noticeable in the HT-29 cell line.

The only deviation from the synergistic trend of S1/2/3/4 was observed at the lowest 0.5 μM verapamil concentration that exhibited a modest antagonistic joint effect with doxorubicin in HL-60/Dox cells, probably as a result of urged P-gp ATP-ase activity by low verapamil concentration. However, this phenomenon, was well eliminated in all other combination ratios of S1/2/3/4 with doxorubicin.

In conclusion, the findings of the conducted synergism study show superior chemosensitizing activity of the experimental verapamil-loaded nanocomposites in HT-29 and HL-60/Dox cells, as compared to free verapamil, presumably as a result of a positive efflux pump modulation.

Acknowledgements

Financial support from the Bulgarian National Science Fund (grant ДН 09/18) and the Bulgarian-Hungarian Inter-Academic Exchange Agreement is greatly appreciated.

Appendix A. Supplementary material

Supplementary data to this article can be found online at https://doi.org/10.1016/j.ejpb.2019.07.021.

References

[1] S. Senapati, A.K. Mahanta, S. Kumar, P. Maiti, Controlled drug delivery vehicles for cancer treatment and their performance, Signal Transduct Target Ther. 16 (2018) 3–7.
[2] R. Guillet-Nicolas, J.-L. Bridot, Y. Seo, M.-A. Fortin, F. Kleitz, Enhanced relaxometric properties of MRI "Positive" contrast agents confined in three-dimensional cubic mesoporous silica nanoparticles, Adv. Funct. Mater. 21 (2011) 4653–4662.
[3] M. Manzano, V. Aina, C.O. Arean, F. Balas, V. Cauda, M. Colilla, M.R. Delgado, M. Vallet-Regí, Studies on MCM-41 mesoporous silica for drug delivery: effect of particle morphology and amine functionalization, Chem. Eng. J. 137 (2008) 30–37.
[4] P. Horcajada, A. Ramila, G. Ferey, M. Vallet-Regí, Influence of superficial organic modification of MCM-41 matrices on drug delivery rate, Solid State Sci. 8 (2006) 1243–1249.
[5] X. Huang, L. Li, T. Liu, N. Hao, H. Liu, D. Chen, F. Tang, The shape effect of mesoporous silica nanoparticles on biodistribution, clearance, and biocompatibility in Vivo, ACS Nano 5 (2011) 5390–5399.
[6] a) J. Lu, M. Liong, Z. Li, J.I. Zink, F. Tamanoi, Biocompatibility, biodistribution, and drug-delivery efficiency of mesoporous silica nanoparticles for cancer therapy in animals, Small 6 (2010) 1794–1805;
b) Q. He, J. Shi, F. Chen, M. Zhu, L. Zhang, An anticancer drug delivery system based on surfactant-templated mesoporous silica nanoparticles, Biomaterials 31 (2010) 3335–3346.
[7] S. Habib, F. Launay, H.E. Zakhem, M. Mazaj, F. Guenneau, P. Beaunier, D. Brouri, N. Novak Tusar, V. Kaucic, A. Gedeon, ZSM-5/SBA-15 microporous/mesoporous composites prepared by a microwave-assisted zeolitisation of Al-SBA-15 mesoporous solids, Mater. Res. Bull. 48 (2013) 1288–1295.
[8] W. Xu, X. Gao, P. Ge, F. Jiang, X. Zhang, J. Xie, Dendrimer-like mesoporous silica nanospheres with suitable surface functionality to combat the multidrug resistance, Inter. J. Pharm. Sci. 553 (2018) 349–362.
[9] N. Poonia, V. Lather, D. Pandita, Mesoporous silica nanoparticles: a smart nanosystem for management of breast cancer, Drug Discovery Today 23 (2) (2018) 1–18.
[10] A. Szegedi, M. Popova, I. Goshev, J. Mihály, Effect of amine functionalization of spherical MCM-41 and SBA-15 on controlled drug release, J. Solid State Chem. 184 (2011) 1201–1207.
[11] G.J. Owens, R.K. Singh, F. Foroutan, M. Alqaysi, Ch.-M. Han, Ch. Mahapatra, H.-W. Kim, J.C. Knowles, Sol–gel based materials for biomedical applications, Prog. Mater Sci. 77 (2016) 1–79.
[12] M. Todorova, A. Trendafilova, K. Danova, D. Dimitrov, Phytochemical study of Anthemis rumelica (Velen.) Stoj. & Acht, Biochem. Syst. Ecol. 39 (4–6) (2011) 868–871.
[13] P. Dong, K.P. Rakesh, H.M. Manukumar, Y.H.E. Mohammede, C.S. Karthikd, S. Sumathif, P. Mallud, Hua-Li Qina, Innovative nano-carriers in anticancer drug delivery – a comprehensive Review, Bioorg. Chem. 85 (2019) 325–336.
[14] a) E. Beck, W.J. Sieber, R. Trejo, Am Fam Phys. 71 (2005) 717;
b) A.J. Giannini, R.S. Tarasewski, R.H. Loiselle, Verapamil and lithium in maintenance therapy of manic patients, J. Clin. Pharmacol. 27 (1987) 980–982.
[15] C. Rustichelli, M.C. Gamberini, V. Ferioli, G. Gamberini, Properties of the racemic species of verapamil hydrochloride and gallopamil hydrochloride, Inter. J. Pharm. 178 (1999) 111–120.
[16] J.G. jr Clothier, S.A. Tomellini, Chiral separation of verapamil and related compounds using micellar electrokinetic capillary chromatography with mixed micelles of bile salt and polyoxyethylene ethers. J. Chromatogr. A 723 (1996) 179–187.
[17] K.M. Pluchino, M.D. Hall, Andrew S. Goldsborough, Richard Callaghan, Michael M. Gottesman, Collateral sensitivity as a strategy against cancer multidrug resistance, Drug Resist Updat. 15 (1–2) (2012) 98–105.
[18] H. Afrooz, F. Ahmadi, F. Fallahzadeh, S.H. Mousavi-Fard, Sh. Alipour, Design and characterization of paclitaxel-verapamil co-encapsulated PLGA nanoparticles: potential system for overcoming P-glycoprotein mediated MDR, J. Drug Delivery Sci. Technol. 41 (2017) 174–181.
[19] Ch.-P. Wu, Ch.-H. Hsieh, Y.-Sh. Wu, The emergence of drug transporter-mediated multidrug resistance to cancer chemotherapy, Mol. Pharmaceutics 8 (6) (2011) 1996–2011.
[20] X.H. Vu, U. Bentrup, M. Hunger, R. Kraehnert, U. Armbruster, A. Martin, Direct synthesis of nanosized-ZSM-5/SBA-15 analog composites from preformed ZSM-5 precursors for improved catalytic performance as cracking catalyst, J. Mater. Sci. 49 (2014) 5676–5689.
[21] a) T. Chou, Theoretical basis, experimental design, and computerized simulation of synergism and antagonism in drug combination studies. (2007) 621–681; b) T.C. Chou, Drug combination studies and their synergy quantification using the choutalalay method, Cancer Res. 70 (2010) 440–446.
[22] Gaussian 09, Revision D.01, M.J. Frisch, G.W. Trucks, H.B. Schlegel, G.E. Scuseria, M.A. Robb, J.R. Cheeseman, G. Scalmani, V. Barone, B. Mennucci, G.A. Petersson, H. Nakatsuji, M. Caricato, X. Li, H.P. Hratchian, A.F. Izmaylov, J. Bloino, G. Zheng, J.L. Sonnenberg, M. Hada, M. Ehara, K. Toyota, R. Fukuda, J. Hasegawa, M. Ishida, T. Nakajima, Y. Honda, O. Kitao, H. Nakai, T. Vreven, J.A. Montgomery Jr., J.E. Peralta, F. Ogliaro, M. Bearpark, J.J. Heyd, E. Brothers, K.N. Kudin, V.N. Staroverov, R. Kobayashi, J. Normand, K. Raghavachari, A. Rendell, J.C. Burant, S. S. Iyengar, J. Tomasi, M. Cossi, N. Rega, J.M. Millam, M. Klene, J.E. Knox, J.B. Cross, V. Bakken, C. Adamo, J. Jaramillo, R. Gomperts, R.E. Stratmann, O. Yazyev, A.J. Austin, R. Cammi, C. Pomelli, J.W. Ochterski, R.L. Martin, K. Morokuma, V.G. Zakrzewski, G.A. Voth, P. Salvador, J.J. Dannenberg, S. Dapprich, A.D. Daniels, Ö. Farkas, J.B. Foresman, J.V. Ortiz, J. Cioslowski, D.J. Fox, Gaussian, Inc., Wallingford CT, 2009.
[23] Y. Zhao, D.G. Truhlar, The M06 suite of density functionals for main group thermochemistry, thermochemical kinetics, noncovalent interactions, excited states, and transition elements: two new functionals and systematic testing of four M06-class functionals and 12 other functionals, Theor. Chem. Acc. 120 (2008) 215–241.
[24] J. Tomasi, B. Mennucci, R. Cammi, Quantum mechanical continuum solvation models, Chem. Rev. 105 (2005) 2999–3093.
[25] T.H. Chen, B.H. Wouters, P.J. Grobet, Aluminium coordinations in zeolite mordenite by ^{27}Al multiple quantum MAS NMR spectroscopy, Eur. J. Inorg. Chem. 281–285 (2000).
[26] Z. Wang, Y. Jiang, O. Lafon, J. Trebosc, K.D. Kim, Catherine Stampfl, Alfons Baiker, Jean-Paul Amoureux, Jun Huang, Brønsted acid sites based on penta-coordinated aluminum species, Nat. Commun. 7 (2016) Article number: 13820.
[27] B. Marler, U. Oberhagemann, S. Vortmann, H. Gies, Influence of the sorbate type on the XRD peak intensities of loaded MCM-411, Microporous Mater. 6 (1996) 375–383.
[28] I.B. Cozar, L. Szabo, N. Leopold, V. Chis, O. Cozar, L. David, IR, Raman, SERS and DFT study of pindolol and verapamil, J. Mol. Struc. 993 (2011) 308–315.
[29] Y. Chang, S.F. Chen, Z. Zhang, S.Y. Jiang, Highly protein-resistant coatings from well-defined diblock copolymers containing sulfobetaines, Langmuir 22 (2006) 2222–2226.
[30] S.Y. Jiang, Z.Q. Cao, Ultralow-fouling, functionalizable, and hydrolysable zwitterionic materials and their derivatives for biological applications, Adv. Mater. 22 (2010) 920–932.
[31] S.P. Duddu, D.J.W. Grant, Formation of the racemic compound of ephedrine base from a physical mixture of its enantiomers in the solid, liquid, solution, or vapor state, Pharm. Res. 9 (1992) 1083–1091.
[32] W. Zhenga, M. Lib, Y. Linc, X. Zhan, Encapsulation of verapamil and doxorubicin by MPEG-PLA to reverse drug, resistance in ovarian cancer, Biomed. Pharmacother. 108 (2018) 565–573.